

# MAGNETIC FIELD ANALYSIS OF A PLANAR SUPERCONDUCTING UNDULATOR WITH VARIABLE FIELD POLARIZATIONS\*

S.H. Kim<sup>†</sup> and C. Doose

Advanced Photon Source, Argonne National Laboratory  
9700 S. Cass Ave., Argonne, IL 60439, USA

## Abstract

A planar superconducting undulator (SCU), which generates horizontal and vertical fields,  $B_x$  and  $B_y$ , perpendicular to the beam directions, is inserted in between the magnetic poles of another unit, which generates the vertical field  $B_y$ . Analytical formulae of the magnetic fields are presented for the inserted, as well as the vertical-field, units. A scaling law may be applied to the SCU. The angle of the coil windings for the inserted unit is analyzed to maximize  $B_x$ . The range of the optimum rotation angle, for the range of gap/period ratio 0.1 – 0.6, is calculated to be  $30^\circ - 40^\circ$ .

## INTRODUCTION

A planar-type superconducting undulator (SCU) with the current of the coil in the x-direction generates vertical and horizontal fields,  $B_y$  and  $B_z$ . In the midplane of the undulator,  $B_z$  for the top and bottom coils cancels out, and only  $B_y$  remains. A helical field in the midplane of a planar undulator may be expressed as

$$B = B_y \sin\left[\frac{2\pi}{\lambda} z\right] + B_x \sin\left[\frac{2\pi}{\lambda} \left(z \pm \frac{\lambda}{4}\right)\right], \quad (1)$$

where  $\lambda$  is the magnetic period length along the electron-beam direction on the z-axis. The device requires an additional component of the current other than in the x-direction for the horizontal field  $B_x$ . Figure 1 shows a schematic planar-type undulator with superconducting (SC) coils to produce the variable helical field described by Eq. (1). The SCU consists of two units, the outer and the inserted units. The outer unit generates the vertical field  $B_y$  in the midplane. The inserted unit, which is located in between the pole gap of the outer unit, generates both the horizontal and vertical fields,  $B_x$  and  $B_y$ , in the midplane. The top and bottom coils for the inserted unit are rotated in opposite directions by an angle  $\phi$  around the vertical axis.

The main advantage of the planar-type SCU is that, unlike double-helix coil windings on a cylindrical beam tube, it can be designed to have a large horizontal aperture. Also, by changing the operating currents and their directions, independently for the two units, different polarizations of the photon beams may be generated. The idea of rotating the coils was first proposed by Walker [1]

and later by Sasaki [2]. Rossmanith and his coworkers demonstrated the tunability of the magnetic field with a superimposed vertical field [3]. Steel magnetic poles and flux-return yokes may be used for the outer unit to enhance the vertical field and to confine the stray field [4]. In this paper, the magnetic field for the outer unit without any steel is expressed. Then, the analytical formulae of the magnetic field for the inserted unit are derived. The optimum rotation angle for the inserted unit is also calculated to maximize the horizontal field  $B_x$ .

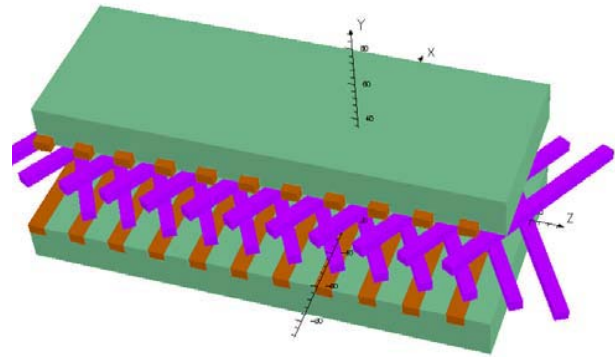


Figure 1: A schematic planar-type undulator with SC coils to produce a variable helical field. An elliptical-field unit is inserted in between the pole gap of an outer vertical-field unit.

## THE OUTER VERTICAL-FIELD UNIT

The outer unit has a magnetic period length  $\lambda$  along the z-axis and a pole gap of  $h$ . The coils have cross sections of  $(c \times d)$  with  $d$  as the height and average current densities of  $+j$  and  $-j$ . For an infinitely long device, the current density  $J_x$  for a unit height of the coil may be expressed in a Fourier series:

$$J_x(z) = \sum_{n=1}^{\infty} \frac{4j}{n\pi} \sin^2\left(\frac{n\pi}{2}\right) \sin\left(nk \frac{c}{2}\right) \cos(nkz), \quad (2)$$

where  $k = 2\pi/\lambda$ . The vector potential in the pole gap region is given by

$$A_x(y, z) = \sum_{n=1,3,\dots} \frac{-1}{nk} B_n^o \cos(nkz) \exp(\pm nky), \quad (3)$$

$$\text{with } B_n^o = \frac{\mu_0 j \lambda}{(n\pi)^2} \sin\left(nk \frac{c}{2}\right) [e^{-nkh/2} - e^{-nk(h/2+d)}], \quad (3a)$$

where the upper/lower signs in Eq. (3) are for the upper/lower coils of the unit, respectively, and  $\mu_0$  is the magnetic permeability in free space. From the vector

\*Work supported by the U.S. Department of Energy under Contract No. W-31-ENG-38.

<sup>†</sup>shkim@aps.anl.gov

potential  $A_x$ , the field components  $B_y$  and  $B_z$  in the pole gap region are calculated as [5]:

$$B_y = \sum_{n=1,3,\dots} 2B_n^o \sin(nkz) \cosh(nky), \quad (4a)$$

$$B_z = \sum_{n=1,3,\dots} 2B_n^o \cos(nkz) \sinh(nky). \quad (4b)$$

The magnitude of the field, which may be calculated from the above equations, must be superimposed on that of the inserted coils to limit the critical current density.

## THE INSERTED UNIT

Figure 2 shows a top view of the rotated coils for the inserted unit. It has a period length of  $\lambda_z$  in the  $z$ -direction and  $\lambda_0$  before the rotation. The period  $\lambda_z$  should be chosen to be the same as the period  $\lambda$  for the outer unit. The inserted unit has a pole gap of  $g$ , coil cross sections of  $(a \times b)$  with  $b$  as the height, and average current densities of  $+j_0$  and  $-j_0$ . As stated earlier, the upper and lower coils are rotated, respectively, by angles  $+\phi$  and  $-\phi$  around the vertical axis. The rotation of the coils decomposes the current density  $j_0$  into  $j_{0x} = j_0 \cos \phi$  and  $j_{0z} = \pm j_0 \sin \phi$ . It is clear that the rotation does not change the field coefficient for the rotated coils corresponding to Eq. (3a). Hence, from Eq. (3), we may write the vector potentials for the rotated coils:

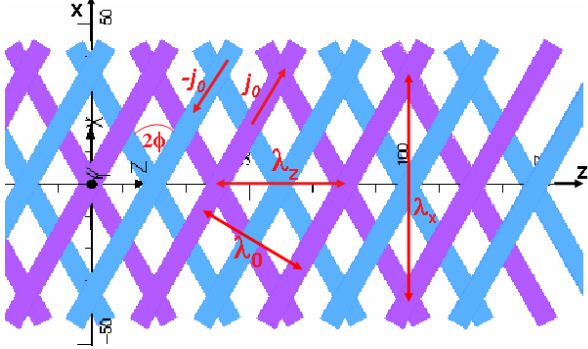


Figure 2: Top view of the rotated coils of the inserted unit. Arrows on the coils indicate the current directions.

$$A_x(x, y, z) = \cos \phi \sum_{n=1,3,\dots} \frac{-1}{nk_0} B_n \cos(nk_z z \mp nk_x x) \exp(\pm nk_0 y),$$

$$A_z(x, y, z) = \mp \sin \phi \sum_{n=1,3,\dots} \frac{-1}{nk_0} B_n \cos(nk_z z \mp nk_x x) \exp(\pm nk_0 y),$$

$$\text{with } B_n^i = \frac{\mu_0 j_0 \lambda_0}{(n\pi)^2} \sin(nk_0 \frac{a}{2}) [e^{-nk_0 g/2} - e^{-nk_0 (g/2+b)}], \quad (6)$$

where  $k_0 = 2\pi / \lambda_0$ ,  $k_x = 2\pi / \lambda_x$ , and  $k_z = 2\pi / \lambda_z$ . The upper/lower signs in the equations are for the upper/lower coils, respectively. As shown in Fig. 2, the undulator periods in the  $x$  and  $z$  directions are determined by the rotating angle  $\phi$ :

$$\lambda_x = \lambda_0 / \sin \phi, \quad \lambda_z = \lambda_0 / \cos \phi. \quad (7)$$

From the above two vector potentials, the magnetic fields for  $|y| < g/2$  are given by

$$B_x = \sin \phi \sum_{n=1,3,\dots} B_n^i \cos(nk_z z \mp nk_x x) \exp(\pm nk_0 y), \quad (8a)$$

$$B_y = \sum_{n=1,3,\dots} B_n^i \sin(nk_z z \mp nk_x x) \exp(\pm nk_0 y), \quad (8b)$$

$$B_z = \pm \cos \phi \sum_{n=1,3,\dots} B_n^i \cos(nk_z z \mp nk_x x) \exp(\pm nk_0 y), \quad (8c)$$

where the upper/lower signs in the equations are for the upper/lower coils, respectively. It is seen from Eq. (8) that, along the  $z$ -direction at  $x = \pm \lambda_x/4$  and  $y = 0$ , where the current directions of the top and bottom coils are in the opposite directions,  $B_z$  is the only nonvanishing field. When the  $z$ -axis in Fig. 2 is chosen as the undulator axis, the fields on the axis are given by

$$B_x = \sin \phi \sum_{n=1,3,\dots} 2B_n^i \cos(nk_z z), \quad (9a)$$

$$B_y = \sum_{n=1,3,\dots} 2B_n^i \sin(nk_z z), \quad (9b)$$

which shows that the inserted unit is a device for a fixed helical field.

## THE ROTATION ANGLE

When the angle  $\phi$  is increased to increase  $j_0 \sin \phi$ , the period  $\lambda_0$  must be started with a smaller value to have an intended period  $\lambda_z$  in the  $z$ -direction, which, in turn, reduces the field for a given pole gap. Hence, an angle  $\phi$  may be chosen to maximize  $B_x$ . From Eq. (8a), the magnitude of  $B_x$  is approximately given by

$$|B_x| \approx \sin \phi \frac{2\mu_0 j_0 \lambda_0}{\pi^2} \sin\left(\frac{\pi a}{\lambda_0}\right) [e^{-\pi g/\lambda_0} - e^{-\pi(g+2b)/\lambda_0}], \quad (10)$$

with  $\lambda_0 = \lambda_z \cos \phi$ . With  $a/\lambda_0 = 0.333$ ,  $b/\lambda_0 = 0.2755$ , and  $\lambda_z = 23.1$  mm, for example, the horizontal field  $B_x$  at a current density of  $1 \text{ kA/mm}^2$  is plotted in Fig. 3 as a function of the angle  $\phi$  and  $g/\lambda_z$  ratio. The figure shows that the optimum angle, which gives the maximum  $B_x$ , depends on the  $g/\lambda_z$ . Figure 4 plots the optimum angle as a function of the  $g/\lambda_z$ . Also plotted in the figure is the fraction of  $B_x$  at  $30^\circ$  to that at the optimum angle. For  $g/\lambda_z > 0.25$ , for example, a  $30^\circ$  rotation of the coils gives  $B_x$  higher than 97% of the possible maximum values.

For the parameters for Fig. 4,  $\lambda_0 = 20$ ,  $a = 6.66$ ,  $b = 5.51$  (all in mm units), and  $\phi = 30^\circ$ , the inserted unit generates a helical field of  $B_x/B_y = 0.5$  with  $\lambda_z = 23.1$ . From a 3-D model with a width of the inserted unit 76 mm in the  $x$ -direction, the elliptical fields for  $j_0 = 1 \text{ kA/mm}^2$  and  $g/\lambda_z = 0.4$  are plotted in Fig. 5. For the end field, the current densities for the last three coil grooves were reduced to 0.85, 0.5 and 0.15 of  $j_0$ . With the width of the coil 76 mm, the numerical data for Fig. 5 agree with Eq. (9), indicating that the width is wide enough. Figure 6

shows the design of an aluminum core for 30°-rotated coil windings of the inserted unit.

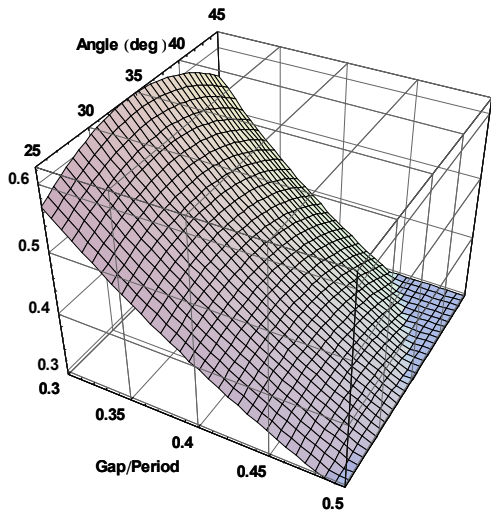


Figure 3: The horizontal field  $B_x$  (vertical axis), per unit current density (kA/mm<sup>2</sup>), depends on the coil rotation angle  $\phi$  and gap/period ratio  $g/\lambda_z$ . The field is calculated for  $a/\lambda_0 = 0.333$ ,  $b/\lambda_0 = 0.2755$ , and  $\lambda_z = 23.1$  mm. The optimum angle shifts from about 34° to 30° when  $g/\lambda_z$  changed from 0.3 to 0.5.

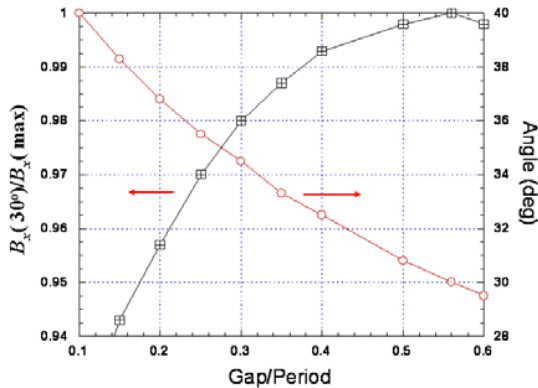


Figure 4: For the same parameters used for Fig. 3, the optimum rotation angle  $\phi$  and the ratio of  $B_x$  at 30° and  $B_x(\text{max})$  at the optimum angle are plotted.

### CONCLUDING REMARKS

From Eqs. (3a) and (6), it is seen that the magnetic fields remain unchanged, for a constant value of  $j\lambda$  or  $j_0\lambda_0$ , when the ratios of the coil dimensions and pole gap to the period remain unchanged. The scaling law also holds for the nonlinear case when soft iron poles, instead of air ones, are used to enhance the vertical field for the outer unit [5].

Since the outer unit requires an additional pole gap for the inserted unit and the vertical field is a function of  $e^{-\pi g/\lambda}$ , there is a lower limit for the period, in a practical sense, to achieve the full range of the field polarization.

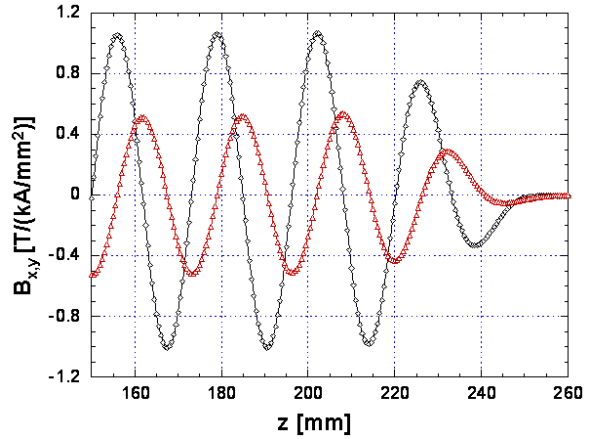


Figure 5: Elliptical fields,  $B_x/B_y = 0.5$ , are plotted from calculations of a 3-D model with parameters:  $a = 6.66$ ;  $b = 5.51$ ;  $g = 8.1$ ;  $\lambda_z = 23.1$ ; width in the x-direction = 76 (all in mm units); and  $\phi = 30^\circ$ .

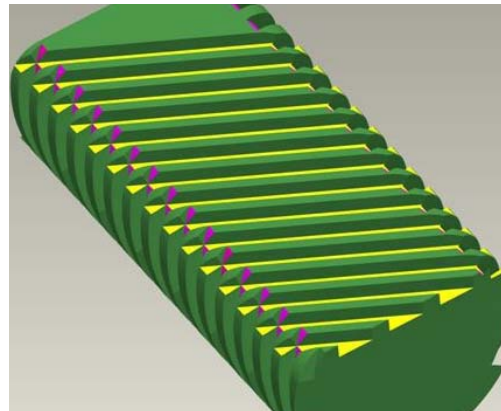


Figure 6: A core for coil winding grooves of  $\phi = 30^\circ$  is designed for the inserted unit. Part of the conductor-return grooves are shown on the curved side.

### REFERENCES

- [1] R.P. Walker, "New Concept for a Superconducting Planar Helical Undulator," ELETTRA Internal Report, Oct. 2000.
- [2] S. Sasaki, "Design of a Superconducting Planar Helical Undulator," Proc. Workshop on Superconducting Undulators and Wigglers, ESRF, Grenoble, June 2003.
- [3] R. Rossmannith et al., "Superconductive Undulators with Variable Polarization Direction," 2004 ASC, Jacksonville, Florida, Oct. 2004.
- [4] S.H. Kim et al., "Experimental Study of the Stability Margin with Beam Heating in a Short-Period Superconducting Undulator for the APS," EPAC 2004, Lucerne, Switzerland, July 5-9, 2004.
- [5] S.H. Kim, "A Scaling Law for the Magnetic Field of Superconducting Undulators," Nucl. Instrum. Methods A, to be published.